Solar Energy Materials and Solar Cells
Volume 95, Issue 10, October 2011, Pages 2831-2836
doi:10.1016/j.solmat.2011.05.044 | How to Cite or Link Using DOI
Permissions & Reprints

Organic photovoltaic devices with a crosslinkable polymer interlayer

Nam Su Kang[a, c], Byeong-Kwon Ju[a], Tae Wan Lee[b], Dong Hoon Choi[b], , , Jae-Min Hong[c] and Jae-Woong Yu[d], ,

[a] Display and Nanosystem Laboratory, College of Engineering, Korea University, Seoul 136-713, Republic of Korea

[b] Department of Chemistry, Advanced Materials Chemistry Research Center, Korea University, Seoul 136-701, Republic of Korea

[c] Future Convergence Research Division, Korea Institute of Science and Technology, P.O. Box 131, Cheongryang, Seoul 130-650, Republic of Korea

[d] Department of Advanced Materials Engineering for Information and Electronics, Kyung Hee University, Seocheon-dong, Giheung-gu, Yongin, Gyeonggi 446-701, Republic of Korea

Received 29 March 2011; revised 20 May 2011; accepted 22 May 2011. Available online 15 June 2011.

Solar Energy Materials & Solar Cells 95 (2011) 2831–2836

Contents lists available at ScienceDirect

Solar Energy Materials & Solar Cells

journal homepage: www.elsevier.com/locate/solmat

Organic photovoltaic devices with a crosslinkable polymer interlayer

Nam Su Kang [a,c], Byeong-Kwon Ju [a], Tae Wan Lee [b], Dong Hoon Choi [b,*], Jae-Min Hong [c], Jae-Woong Yu [d,*]

[a] Display and Nanosystem Laboratory, College of Engineering, Korea University, Seoul 136-713, Republic of Korea
[b] Department of Chemistry, Advanced Materials Chemistry Research Center, Korea University, Seoul 136-701, Republic of Korea
[c] Future Convergence Research Division, Korea Institute of Science and Technology, P.O. Box 131, Cheongryang, Seoul 130-650, Republic of Korea
[d] Department of Advanced Materials Engineering for Information and Electronics, Kyung Hee University, Seocheon-dong, Giheung-gu, Yongin, Gyeonggi 446-701, Republic of Korea

ARTICLE INFO

Article history:
Received 29 March 2011
Received in revised form
20 May 2011
Accepted 22 May 2011
Available online 15 June 2011

Keywords:
Organic photovoltaic
Polymer solar cell
Curable interlayer
Current extraction
Fill factor

ABSTRACT

Organic photovoltaic devices with a photo-crosslinkable interlayer were fabricated. This photo-crosslinkable interlayer acted as a leakage current reducing buffer layer. The performance of the small area OPV cell (0.04 cm^2) was enhanced by the increase in the short circuit current and the fill factor. When a larger area cell (1 cm^2) was used, the performance of OPV cell increased when the appropriate interlayer thickness was used. In the case of a 10 cm × 10 cm module, the power conversion efficiency was about double than that without the interlayer. The insertion of the interlayer increased the current extraction by lowering the barrier height and attenuated the fill factor reduction by enhancing the rectification with a better leakage current sealing. From this study, it is clearly proved that the insertion of the appropriate photo-crosslinkable layer improves the performance of OPV devices, the effect was especially evident for large area cells.

1. Introduction

Organic photovoltaics (OPVs) have received growing attentions because they have several advantages over traditional silicon-based or other inorganic solar cells, such as their excellent processability, light weight, and their capability to form large area devices at a low cost [1–10]. An efficient bicontinuous interpenetrating network structure, which can produce high conversion efficiency, can be easily obtained by the simple spin coating of a polymer blend solution [11–15]. Therefore, OPVs have the potential to provide low cost solar power conversion methods. Recent improvement of the power conversion efficiency utilizing bulk heterojunction interpenetrating network structures, low band gap materials, and advanced device fabrication methods (tandem cells, inverted cells, and parallel or series connections, etc.) draw great anticipation for commercial OPV devices in the near future [9,16–21]. Nonetheless, the conversion efficiency of OPV devices hitherto attainable is still not close to the approximate maximum value of 11% [22–25]. The best advantage of OPV is that it can be fabricated in a flexible form by printing technology. Recently many researchers have been focused on utilization of roll-to-roll processing to reduce the production cost [26,27].

Because of the relatively low conversion efficiency of OPV devices, they need a large scale photoactive area to achieve the desired power output [28,29]. However, the performance of a single OPV cell decreases with an increase in the active area because of the high resistivity caused by the increase in series resistance and the decrease in the fill factor. A close relationship between the device area and the conversion efficiency is now well established. In order to achieve the maximum power conversion efficiency for a large active area device, it is important to maintain the fill factor as the active area increases or at least minimize the reduction of the fill factor. A buffer layer has been used to attenuate this fill factor loss [30]; however, the solution processed overlaid structure forming the preparation characteristics of the OPV limits the use of high quality semiconductors because of the similarity in the solubility of the solvents used. One way of solving the problem for forming multi-layer structure was the utilization of insoluble polythiophene, which was prepared by the precursor method using thermo-cleavable side chains [31,32].

In this work, we focus our efforts on using a photo-crosslinkable precursor as a buffer layer and study the influence of this interlayer on the device performance in terms of the short circuit current, the open circuit voltage, and the fill factor. The utilization of this crosslinkable interlayer allows a layer by layer processing of the solution coating technique. This method provides a distinct implementation advantage by using simple printing techniques, such as inkjet, gravure, offset and screen lithography, and soft contact transfer in the future application of printed electronics.

2. Materials and methods

2.1. Synthesis and basic characterization of photo curable precursor (T43)

1″,1′,1-2,2′,2″-(3,3′,3″-(1E,1′E,1″E)-2,2′,2″-(benzene-1,3,5-triyl) tris(ethene-2,1-diyl)tris(9H-carbazole-9,3-diyl))tris(ethane-2,1-diyl)

* Corresponding authors. Tel.: +82 31 201 3325; fax: +82 31 204 8114.
E-mail addresses: dhchoi8803@korea.ac.kr (D.H. Choi), jwyu@khu.ac.kr (J.-W. Yu).

0927-0248/$ - see front matter © 2011 Elsevier B.V. All rights reserved.
doi:10.1016/j.solmat.2011.05.044

4-tri(penta-1,4-dien-3-yl) tributanedioate to a solution of 1 (0.392 g, 0.5 mmol) and 2 (0.368 g, 2 mmol) in 40 mL of DCM/THF (1:1) was added to 4-(dimethyl-amino)pyridinium p-toluenesulfonate (DPTS) (0.588 g, 2 mmol) and the mixture was allowed to stir at room temperature under nitrogen atmosphere for 15 min. N,N′-Dicyclohexylcarbodiimide (DCC, 0.412 g, 2 mmol) was then added and the mixture was allowed to stir at room temperature overnight. The reaction mixture was filtered and the filtrate was concentrated under a reduced pressure. The crude product was then purified by silicagel column chromatography (eluent; ethyl acetate/$CHCl_3$=1:20) to obtain 0.55 g of a pure solid: yield 86%.

^{1}H NMR (400 MHz, $CDCl_3$): d(ppm) 8.30 (s, 3H), 8.16 (d, J=8.0 Hz, 3H), 7.76 (d, J=8.0 Hz, 3H), 7.67(s, 3H), 7.47 (m, 12H), 7.28 (m, 6H), 5.82 (m, 6H), 5.72 (t, 3H), 5.26 (m, 12H), 4.59(t, 6H), 4.52 (t, 6H), 2.56 (t, 12H).

^{13}C NMR (100 MHz, $CDCl_3$): d(ppm) 172.30, 171.32, 141.00, 140.44, 138.70, 135.02, 130.01, 129.31, 126.46, 126.29, 124.92, 123.67, 123.31, 120.76, 119.81, 119.03, 117.87, 109.06, 108.95, 75.70, 62.63, 41.93, 29.30, 29.12.

HR-FAB MS m/z: calcd $C_{81}H_{75}N_3O_{12}$ 1281.5351; found 1281.5353 Anal. Calcd: C, 75.86; H, 5.89; N, 3.28. Found: C, 75.39; H, 5.25; N, 3.41.

2.2. The device fabrication

A PEDOT:PSS (poly(3,4-ethylene dioxythiophene)):poly(styrene sulfonate) aqueous dispersion (CLEVIOUS® PH-500) stock solution was spincoated in air at 2000 rpm for 40 s to form an about 35 nm thick film, then film was baked at 200 °C for 10 min in a high purity nitrogen environment glove box. The ITO glass was cleaned by boiling in chloroform, isopropyl alcohol, and acetone for 30 min in each solvent, then sonified for 15 min in a 50:50 isopropyl alcohol and acetone solution, and finally rinsed with deionized water. 0.3 wt% of a photo curable precursor (T43) in chlorobenzene was spincoated onto the ITO/PEDOT substrate; this interlayer was crosslinked by a 256 nm ultraviolet lamp with an intensity of 5 mJ at room temperature for 3 min.

A typical example of the sample preparation is as follows: 4.3 wt% of P3HT (purchased from Rieke Metals, EE grade) and PCBM (purchased from Nano-C) blend with a 1:0.6 ratio by weight was dissolved in anhydrous chlorobenzene and spincoated onto prepared PEDOT:PSS coated ITO glass with/without an interlayer at 2500 rpm for 40 s. The thickness of the resulting active layer was 220 nm; it was pre-annealed at 150 °C for 10 min. 0.8 nm thick LiF, which serves as a buffer layer for electron extraction, was deposited on top of the active layer and a 150 nm thick aluminum layer was evaporated by thermal vapor deposition at 10^{-6}–10^{-7} Torr; the prepared device was post annealed at 120 °C for 10 min. All of the processing was performed in a glove box with a high purity nitrogen environment. The active cell areas were 0.04 cm^2 for the small area, 1 cm^2 for the large area, and 36.4 cm^2 for the largest area module.

2.3. Characterization

The thickness of the coated film was measured with a surface profiler (TENCOR®, P-10 α-step). The surface morphology of the samples was studied using a tapping mode atomic force microscope (Digital Instruments Multimode) equipped with a nanoscope IIIa controller. The absorption spectra of the films were obtained using a photodiode array type UV–Vis spectrometer (HP 8453). An Oriel Class A type solar simulator (IEC 904) with an Oriel Reference Cell (calibrated data traceable to NREL) was used as a light source; all of the measurements were performed under a 1 sun condition (AM 1.5 100 mW/cm^2). The measurements were not corrected for reflection losses and for light absorption in the ITO electrode. The I–V characteristics were determined with a Keithley 2400 source-measure unit.

3. Results and discussions

The chemical structure of the photo curable precursor used in this study is given in Fig. 1(a). This crosslinkable precursor was designed to possess carbazole moieties for a high hole transporting characteristic and pentadienyl moieties for photo-crosslinking sites. UV–Vis spectral changes due to cure process are shown in Fig. 1(b). The decrease in 300 and 350 nm represents the disappearance of the double bond in pentadiene photoreactive groups. In order to study its effectiveness as a buffer layer, the energy levels (HOMO, LUMO, and energy band gap) were studied using a cyclicvoltamogram and UV–Vis spectroscopy. The band energy diagrams are given in Fig. 2. The HOMOs of the photo-crosslinked interlayer material and the P3HT are very close to that of the PEDOT, which serves as a hole extraction layer, so these interlayers can form an ohmic contact with the hole extraction layer. As a result of this ohmic contact, the contact resistance is reduced due to a reduction of the barrier height. Meanwhile LUMOs of interlayer are much bigger than that of P3HT or PCBM, therefore, this interlayer can be acted as an electron blocking layer. Insertion of this electron block layer can improve device performance by reducing separated charge quenching (i.e. electron).

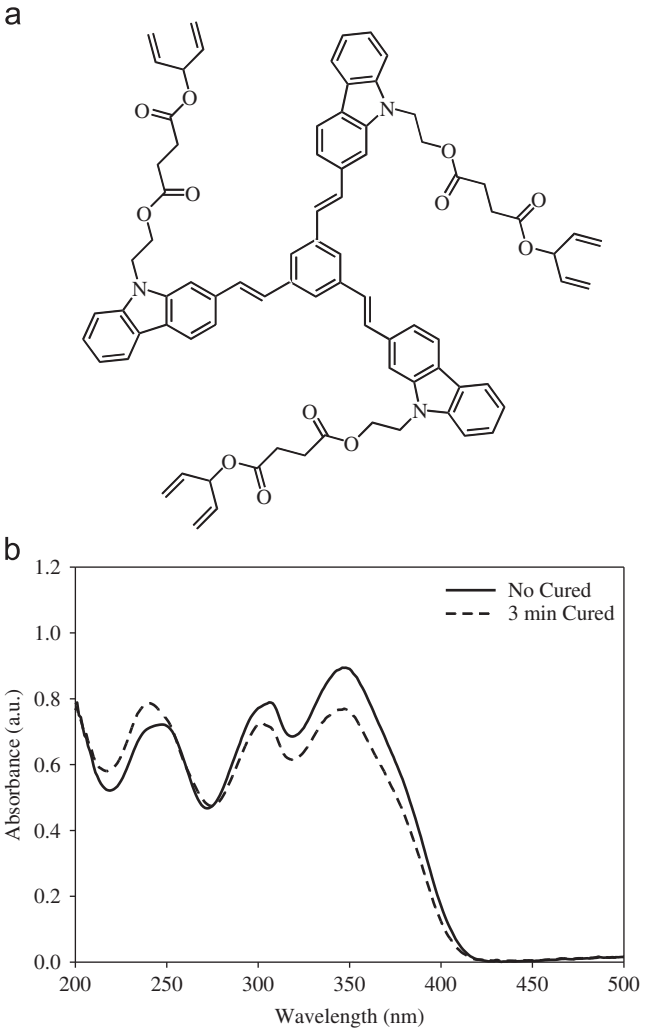

Fig. 1. Chemical structure of the UV crosslinkable polymer.

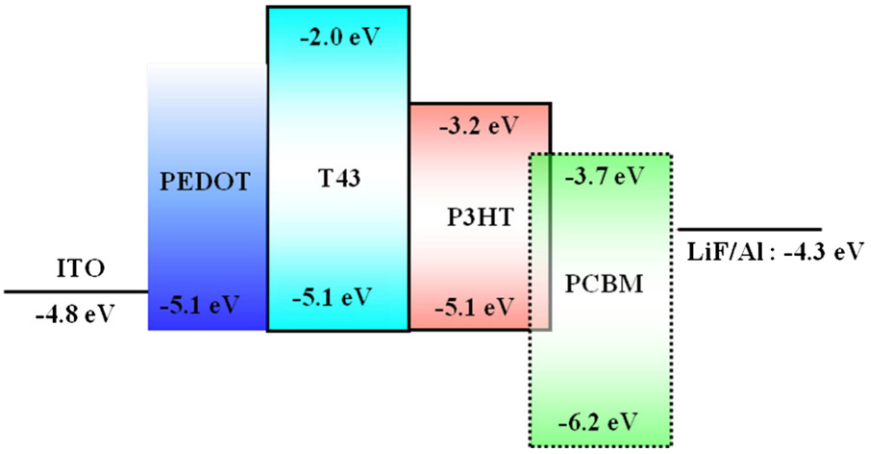

Fig. 2. Band energy diagram.

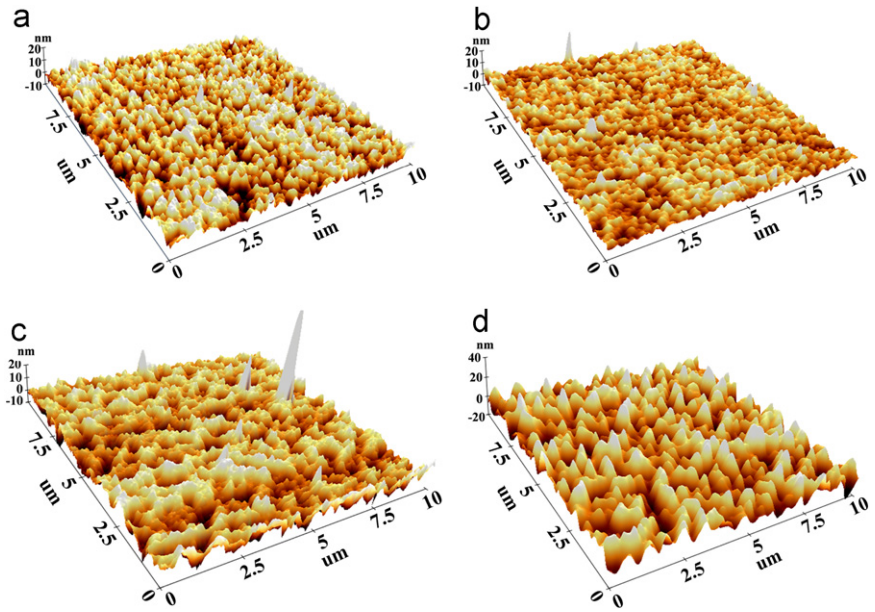

Fig. 3. AFM topography images: (a) ITO, (b) PEDOT on ITO, (c) T43 on PEDOT/ITO and (d) P3HT:PCBM on T43/PEDOT/ITO.

The surface roughness is another important factor affecting the device performance, because OPV devices are made with a very thin (100∼200 nm) active layer. We used AFM to compare the surface roughness of the PEDOT and the interlayer. As shown in Fig. 3, the surface roughness was reduced from ∼3 nm to ∼2 nm when the ITO was coated with the PEDOT (Fig. 3(a) and (b)). After the photo-crosslinking procedure, the surface roughness slightly increased to about 3 nm (Fig. 3(c)). The annealing of the P3HT:PCBM active layer caused a severe deterioration in the surface roughness by about a 10 nm scale. From this image analysis, it was concluded that the photo-cured interlayer would not cause any surface roughness problems. When we compared the AFM images of active layer morphology with and without interlayer, there was not much morphological difference between these two active layers. Therefore, we concluded that the interlayer did not cause any affect on the morphology of active layer and it is understandable since the thickness of the interlayer was only 5 nm thick.

We performed the contact angle study (Krüss DS-100 Drop Shape Analyzer) of the surfaces of the PEDOT and photo-crosslinked interlayer. As shown in Fig. 4, the surface of interlayer is more hydrophobic since the contact angle measurement of PEDOT

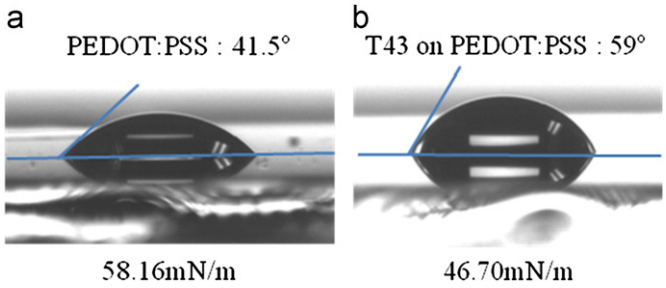

Fig. 4. Contact angle studies: (a) PEDOT surface and (b) interlayer surface.

surface is 41.5° (calculated surface energy is 58.2 mN/m) while that of interlayer is 59° (calculated surface energy is 46.7 mN/m). Utilizing reported surface energy values of PCBM and P3HT [28], of which the surface energy was 37.8 and 26.9, respectively. From these results, it is clear that overlay coating of PCBM:P3HT blend will be more nicely coated on interlayer than PEDOT surface. This better adhesion should help the device performance.

Fig. 5(a) shows the *I–V* characteristics of the small area cell (active area: 0.04 cm^2) with and without the interlayer. The open

circuit voltage, the short circuit current density, the fill factor, and the power conversion efficiency at an AM 1.5 condition without the interlayer (i.e. the reference cell) were, 0.586 V, 8.86 mA/cm^2, 0.649, and 3.38, respectively. When the ~5 nm thick photo-crosslinked interlayer was inserted between the PEDOT and the active layer, their values changed to 0.588 V, 9.96 mA/cm^2, 0.693, and 4.06, respectively. The power conversion efficiency of the device with the interlayer increased by about 20% compared to that of the cell without an interlayer. Fig. 5(b) and (c) show the logarithmic *I–V* characteristics plot of the small area cell (active area: 0.04 cm^2) with and without the interlayer for dark and photo state, respectively. As shown in figures, device with 5 nm thick interlayer showed the lowest dark current while the highest photocurrent. From this plot, it is clear that this interlayer prevented shunt leakage at dark state. The shunt resistance and series resistance of the device measured from *I–V* plot was 6.40×10^4 and 9.78 Ω cm^2 for without the interlayer (reference device) and 2.34×10^5 and 4.86 Ω cm^2 for with interlayer. From these resistances, it is clear that this interlayer is formed by ohmic contact and it also plays role of leakage current preventing layer.

Fig. 6 compares the incident photon to current collection efficiency (IPCE) spectrum of devices with and without the interlayer. The reference device shows the typical spectral response of P3HT:PCBM blend film with a maximum IPCE of ~66% at 516 nm, similar with the other report [33]. For the device with the interlayer, the extracted current was increased due to the interlayer and the maximum IPCE increased to 71% at 516 nm.

The interlayer thickness effects were studied by changing the interlayer thickness; the results are summarized in Table 1. The short circuit current density was increased with a decreasing interlayer thickness, whereas the open circuit voltages were not changed. The devices with and without the interlayer were identical except for the interlayer between the hole extraction layer (PEDOT) and the active layer (all of the devices were prepared under identical conditions), therefore, the difference in the short circuit current and the power conversion efficiency should originate from the decrease in the barrier height between the PEDOT layer and the active layer due to the insertion of the interlayer. The open circuit voltage, which represents the built-in potential in the fabricated devices is mainly determined by the energy difference between the HOMO of the donor material and the LUMO of the acceptor material, which contact to form the heterojunction. Since the device structures were identical with and without the interlayer, and since the HOMO levels of the

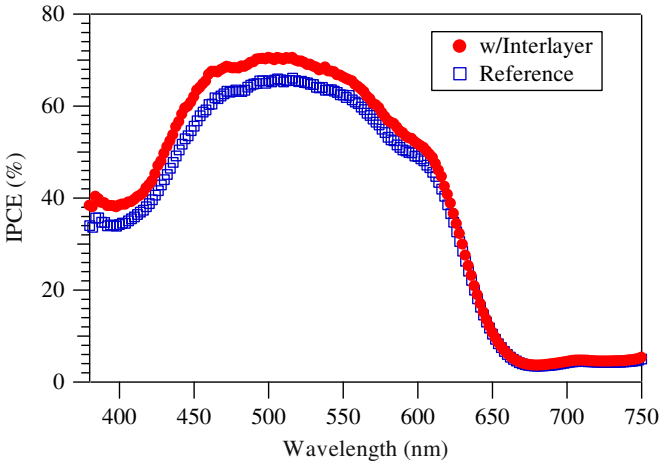

Fig. 6. IPCE plots of the small active area cell (0.04 cm^2) in photo state.

Table 1
Influence of the interlayer thickness on the performance of the OPV devices.

Interlayer thickness (nm)	Open circuit voltage (V)	Short circuit current density (mA/cm^2)	Fill factor	Efficiency
0 (reference)	0.586	8.859	0.649	3.376
52	0.589	9.038	0.669	3.564
26	0.587	9.564	0.657	3.695
12	0.589	9.762	0.654	3.765
5	0.588	9.964	0.693	4.061

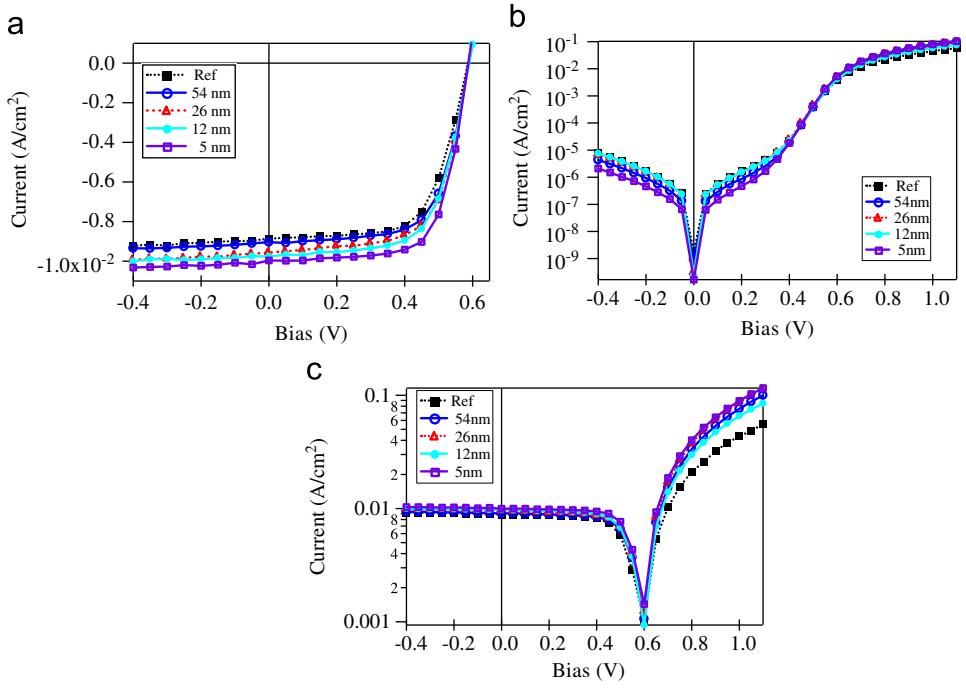

Fig. 5. (a) *I–V* characteristics of the small active area cell (0.04 cm^2), (b) log *I–V* plots of the small active area cell (0.04 cm^2) (dark current), and (c) log *I–V* plots of the small active area cell (0.04 cm^2) (photocurrent).

PEDOT and the interlayer material were very close to each other, the open circuit voltages should not change with the change in the thickness of the interlayer. As shown in Fig. 5(a), the series resistance slightly decreased with a decreasing interlayer thickness, therefore there was a slight increase in the short circuit current density with the decreasing interlayer thickness. The most noticeable change was the fill factor. The shunt resistance representing the rectification of the device was enhanced noticeably, as shown in Fig. 5(a). As a result of this improvement, the fill factor increased from 0.649 for the reference cell to 0.693 for the optimum thickness interlayer, which was about 5 nm thick. From this study, it can be concluded that this photo-crosslinkable interlayer can prevent the flow of leakage current like TiO_X used in an n-type interlayer [25,33].

In order to study the charge transporting characteristics of this interlayer, TFT devices were fabricated to measure the hole mobility within this photo-crosslinked interlayer. The measured hole mobility of the interlayer was 4.81×10^{-3} cm^2/V s, which was very close to or lower than that of the P3HT in the active layer. Therefore it was clear that the short circuit current enhancement was caused by the barrier height reduction of the interlayer. A similar result was reported by Kang et al. [34] in that the short circuit current and the fill factor could be enhanced even with a high resistance hole transporting buffer layer, i.e. polytetrafluoroethylene, if this buffer layer had a low barrier height [35,36].

We applied this interlayer for the cells to a higher active area (i.e. changed the cell area from 0.04 to 1 cm^2). The larger area cells were prepared by the same methods as used for the preparation of the smaller cells. Fig. 7 shows the *I–V* characteristics of the larger cell with and without an interlayer. The open circuit voltage, the short circuit current density, the fill factor, and the power conversion efficiency at an AM 1.5 condition without the interlayer (i.e. the reference cell) were, 0.586 V, 7.587 mA/cm^2, 0.568, and 2.53, respectively. When a 5 nm thick photo-crosslinked interlayer was inserted between the PEDOT and the active layer, their values changed to 0.602 V, 8.644 mA/cm^2, 0.630, and 3.27, respectively. The values of the reference cell were lower than that of the 0.04 cm^2 active area reference cell; it clearly showed that the increment of the active area caused deterioration in the cell performance. Yoo et al. [37] reported that the series resistance increased with an increase in active area using the integrated series connection of several cells. This meant that the performance of the OPV cells was reduced when a larger area cell was used [37,38]. The power conversion efficiency of the device with an interlayer for the larger area cell increased by about 30% compared to the cell without an interlayer. The enhancement of the power conversion efficiency with the interlayer was intensified as the cell area increased. The reduction of the cell performance with an increased cell area was higher without the interlayer (i.e. 3.38–2.53, a 25% reduction), whereas that for the cell with an interlayer was only 20% (i.e. 4.06–3.27). This was caused by the selective diode contact of the interlayer, which led to a better ohmic resistance to the holes and better blocking to the electrons; this effect was enhanced when the active area was increased.

Finally, this interlayer study was applied to a large area 10 cm × 10 cm module, which had active cell area of 36.4 cm^2, as shown in Fig. 8(a). The *I–V* characteristics of these modules are shown in Fig. 8(b). The open circuit voltage, the short circuit current density, the fill factor, and the power conversion efficiency at an AM 1.0 condition without the interlayer (i.e. the reference cell) were, 2.88 V, 1.00 mA/cm^2, 0.271, and 0.78%, respectively. The module with the interlayer was 2.94 V, 1.56 mA/cm^2, 0.296, and 1.36%, respectively. The power conversion efficiency of the module with the interlayer increased by about 2 times compared to that of the cell without an interlayer. As predicted, the performance of the OPV module decreased with an increase in active area because of the high resistivity caused by the increase in the series resistance and a decrease in the fill factor. In order to achieve the maximum power conversion efficiency for a large active area device, it is important to maintain the fill factor as the active area increases. These module experiments clearly showed that the insertion of an interlayer curtailed the reduction of the fill factor. This attenuation of the fill factor

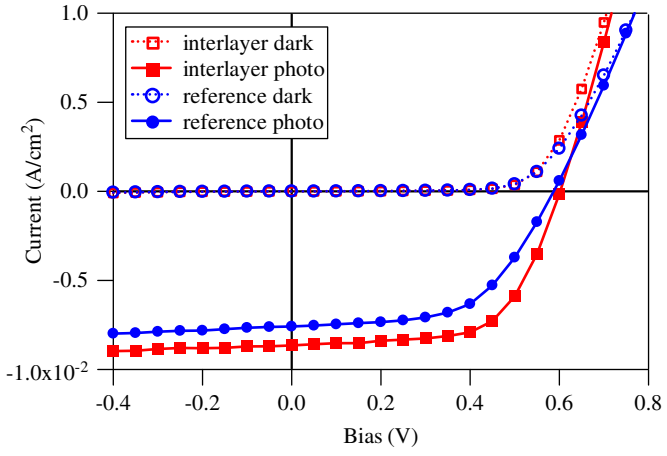

Fig. 7. *I–V* characteristics of the large active area cell (1 cm^2).

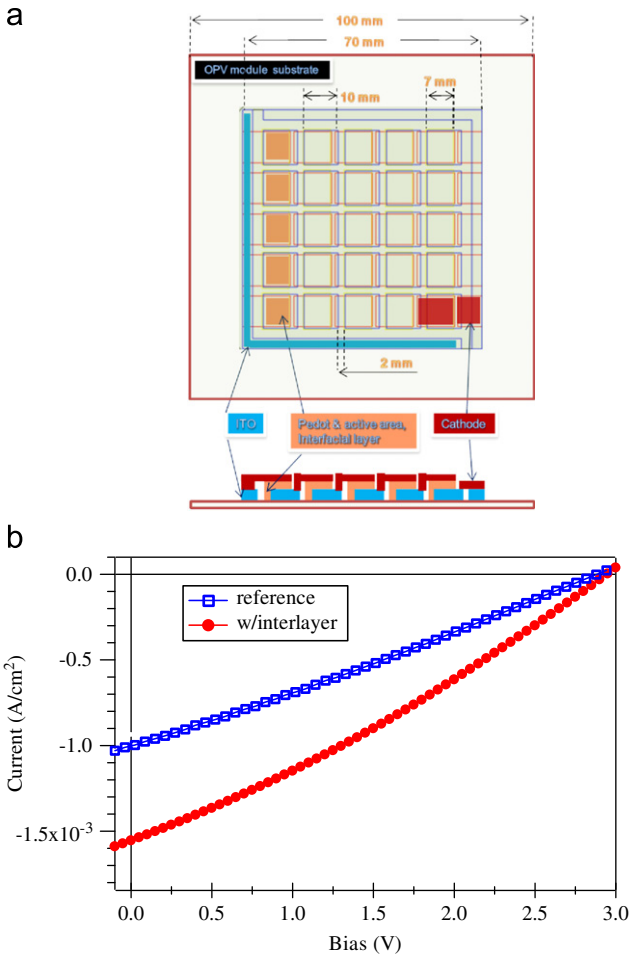

Fig. 8. (a) Schematic diagram of 10 cm × 10 cm module and (b) I–V characteristics of the 10 cm × 10 cm module.

can be achieved by enhancing the rectification with a better leakage current sealing as proved in the increased shunt resistances.

4. Conclusion

In order to maximize the expected capability of OPVs as a future renewable energy source, it is very important to have device fabrication methods suitable for multi-layer printable techniques and an enhanced large area performance. In this study, we used a photo-crosslinkable interlayer, which acts as a buffer layer, not only for a leakage current reducing layer, but also for a multi-layer printable insoluble layer. Since this interlayer is photo-crosslinkable, it can be used in a solution process to form an overlayed structure for polymer semiconductors with a similar organic solvent solubility. This will be an important factor for future organic photovoltaic applications, which will be fabricated using various printing methods with a similar solubility. This interlayer also played an important role in enhancing the rectification and the charge extraction. The influence of the increase in the rectification was severe for modules with a larger active area. In this study, we clearly proved that an insertion of an appropriate photo-crosslinkable layer improved the performance of OPV devices.

Acknowledgments

This research was supported by a Basic Science Research Program through the National Research Foundation of Korea (NRF) funded by the Ministry of Education, Science and Technology (2010-0007122) and by the GRRC program of Gyeonggi province (GRRC Kyung Hee 2010-B03).

References

[1] D. Wohrle, D. Meissner, Organic solar-cells, Adv. Mater. 3 (1991) 129–138.
[2] N.S. Sariciftci, L. Smilowitz, A.J. Heeger, F. Wudl, Photoinduced electron-transfer from a conducting polymer to buckminsterfullerene, Science 258 (1992) 1474–1476.
[3] G. Yu, J. Gao, J.C. Hummelen, F. Wudl, A.J. Heeger, Polymer photovoltaic cells—enhanced efficiencies via a network of internal donor–acceptor heterojunctions, Science 270 (1995) 1789–1791.
[4] J.J.M. Halls, C.A. Walsh, N.C. Greenham, E.A. Marseglia, R.H. Friend, S.C. Moratti, A.B. Holmes, Efficient photodiodes from interpenetrating polymer networks, Nature 376 (1995) 498–500.
[5] C.J. Brabec, N.S. Sariciftci, J.C. Hummelen, Plastic solar cells, Adv. Funct. Mater. 11 (2001) 15–26.
[6] K.M. Coakley, M.D. McGehee, Conjugated polymer photovoltaic cells, Chem. Mater. 16 (2004) 4533–4542.
[7] O. Morton, Solar energy: a new day dawning?: Silicon valley sunrise, Nature 443 (2006) 19–22.
[8] S. Gunes, H. Neugebauer, N.S. Sariciftci, Conjugated polymer-based organic solar cells, Chem. Rev. 107 (2007) 1324–1338.
[9] T. Ameri, G. Dennler, C. Lungenschmied, C.J. Brabec, Organic tandem solar cells: a review, Energy Environ. Sci. 2 (2009) 347–363.
[10] G. Li, V. Shrotriya, Y. Yao, J.S. Huang, Y. Yang, Manipulating regioregular poly(3-hexylthiophene): [6,6]-phenyl-C-61-butyric acid methyl ester blends—route towards high efficiency polymer solar cells, J. Mater. Chem. 17 (2007) 3126–3140.
[11] W.L. Ma, C.Y. Yang, X. Gong, K. Lee, A.J. Heeger, Thermally stable, efficient polymer solar cells with nanoscale control of the interpenetrating network morphology, Adv. Funct. Mater. 15 (2005) 1617–1622.
[12] G. Li, V. Shrotriya, J.S. Huang, Y. Yao, T. Moriarty, K. Emery, Y. Yang, High-efficiency solution processable polymer photovoltaic cells by self-organization of polymer blends, Nat. Mater. 4 (2005) 864–868.
[13] V. Shrotriya, Y. Yao, G. Li, Y. Yang, Effect of self-organization in polymer/fullerene bulk heterojunctions on solar cell performance, Appl. Phys. Lett. 89 (2006) 063505.
[14] Y. Kim, S. Cook, S.M. Tuladhar, S.A. Choulis, J. Nelson, J.R. Durrant, D.D.C. Bradley, M. Giles, I. Mcculloch, C.S. Ha, M. Ree, A strong regioregularity effect in self-organizing conjugated polymer films and high-efficiency polythiophene: fullerene solar cells, Nat. Mater. 5 (2006) 197–203.
[15] M. Campoy-Quiles, T. Ferenczi, T. Agostinelli, P.G. Etchegoin, Y. Kim, T.D. Anthopoulos, P.N. Stavrinou, D.D.C. Bradley, J. Nelson, Morphology evolution via self-organization and lateral and vertical diffusion in polymer: fullerene solar cell blends, Nat. Mater. 7 (2008) 158–164.
[16] J.Y. Kim, K. Lee, N.E. Coates, D. Moses, T.Q. Nguyen, M. Dante, A.J. Heeger, Efficient tandem polymer solar cells fabricated by all-solution processing, Science 317 (2007) 222–225.
[17] H.Y. Chen, J.H. Hou, S.Q. Zhang, Y.Y. Liang, G.W. Yang, Y. Yang, L.P. Yu, Y. Wu, G. Li, Polymer solar cells with enhanced open-circuit voltage and efficiency, Nat. Photon. 3 (2009) 649–653.
[18] L.M. Chen, Z.R. Hong, G. Li, Y. Yang, Recent progress in polymer solar cells: manipulation of polymer: fullerene morphology and the formation of efficient inverted polymer solar cells, Adv. Mater. 21 (2009) 1434–1449.
[19] M.H. Chen, J. Hou, Z. Hong, G. Yang, S. Sista, L.M. Chen, Y. Yang, Efficient polymer solar cells with thin active layers based on alternating polyfluorene copolymer/fullerene bulk heterojunctions, Adv. Mater. 21 (2009) 4238–4242.
[20] J. Jo, S.S. Kim, S.I. Na, B.K. Yu, D.Y. Kim, Time-dependent morphology evolution by annealing processes on polymer: fullerene blend solar cells, Adv. Funct. Mater. 19 (2009) 866–874.
[21] S.Q. Xiao, A.C. Stuart, S.B. Liu, H.X. Zhou, W. You, Conjugated polymer based on polycyclic aromatics for bulk heterojunction organic solar cells: a case study of quadrathienonaphthalene polymers with 2% efficiency, Adv. Funct. Mater. 20 (2010) 635–643.
[22] G. Dennler, M.C. Scharber, C.J. Brabec, Polymer-fullerene bulk-heterojunction solar cells, Adv. Mater. 21 (2009) 1323–1338.
[23] M.C. Scharber, D. Wuhlbacher, M. Koppe, P. Denk, C. Waldauf, A.J. Heeger, C.L. Brabec, Design rules for donors in bulk-heterojunction solar cells—towards 10% energy-conversion efficiency, Adv. Mater. 18 (2006) 789–794.
[24] G. Dennler, M.C. Scharber, T. Ameri, P. Denk, K. Forberich, C. Waldauf, C.J. Brabec, Design rules for donors in bulk-heterojunction tandem solar cells-towards 15% energy-conversion efficiency, Adv. Mater. 20 (2008) 579.
[25] S.H. Park, A. Roy, S. Beaupre, S. Cho, N. Coates, J.S. Moon, D. Moses, M. Leclerc, K. Lee, A.J. Heeger, Bulk heterojunction solar cells with internal quantum efficiency approaching 100%, Nat. Photon. 3 (2009) 297–303.
[26] F.C. Krebs, J. Fyenbo, M. Jørgensen, Product integration of compact roll-to-roll processed polymer solar cell modules: methods and manufacture using flexographic printing, slot–die coating and rotary screen printing, J. Mater. Chem. 20 (2010) 8994–9001.
[27] M. Manceau, D. Angmo, M. Jørgensen, F.C. Krebs, ITO-free flexible polymer solar cells: from small model devices to roll-to-roll processed large modules, Org. Electron. 12 (2011) 566–574.
[28] L. Blankenburg, K. Schultheis, H. Schache, S. Sensfuss, M. Schrodner, Reel-to-reel wet coating as an efficient up-scaling technique for the production of bulk-heterojunction polymer solar cells, Sol. Energy Mater. Sol. Cells 93 (2009) 476–483.
[29] F.C. Krebs, All solution roll-to-roll processed polymer solar cells free from indium-tin-oxide and vacuum coating steps, Org. Electron. 10 (2009) 761–768.
[30] M.D. Irwin, B. Buchholz, A.W. Hains, R.P.H. Chang, T.J. Marks, p-Type semiconducting nickel oxide as an efficiency-enhancing anode interfacial layer in polymer bulk-heterojunction solar cells, Proc. Natl. Acad. Sci. USA 105 (2008) 2783–2787.
[31] O. Hagemann, M. Bjerring, N.C. Nielsen, F.C. Krebs, All solution processed tandem polymer solar cells based on thermocleavable materials, Sol. Energy Mater. Sol. Cells 92 (2008) 1327–1335.
[32] R. Søndergaard, M. Helgesen, M. Jørgensen, F.C. Krebs, Fabrication of polymer solar cells using aqueous processing for all layers including the metal back electrode, Adv. Energy Mater. 1 (2011) 68–71.
[33] J.Y. Kim, S.H. Kim, H.H. Lee, K. Lee, W.L. Ma, X. Gong, A.J. Heeger, New architecture for high-efficiency polymer photovoltaic cells using solution-based titanium oxide as an optical spacer, Adv. Mater. 18 (2006) 572–576.
[34] B.N. Kang, L.W. Tan, S.R.P. Silva, Ultraviolet-illuminated fluoropolymer indium-tin-oxide buffer layers for improved power conversion in organic photovoltaics, Org. Electron. 10 (2009) 1178–1181.
[35] N. Koch, A. Elschner, R.L. Johnson, Green polyfluorene-conducting polymer interfaces: energy level alignment and device performance, J. Appl. Phys. 100 (2006) 024512.
[36] D.S. Germack, C.K. Chan, B.H. Hamadani, L.J. Richter, D.A. Fischer, D.J. Gundlach, D.M. DeLongchamp, Substrate-dependent interface composition and charge transport in films for organic photovoltaics, Appl. Phys. Lett. 94 (2009) 233303.
[37] S. Yoo, W.J. Potscavage, B. Domercq, J. Kim, J. Holt, B. Kippelen, Integrated organic photovoltaic modules with a scalable voltage output, Appl. Phys. Lett. 89 (2006) 233516.
[38] N.S. Kang, B.K. Ju, C. Lee, J.P. Ahn, B.D. Chin, J.W. Yu, Partitioning of the organic layers for the fabrication of high efficiency organic photovoltaic devices, Org. Electron. 10 (2009) 1091–1096.